Dielectric tunability of ferroelectric barium titanate at millimeter-wave frequencies

Charlotte Cochard,[1] Thiemo Spielmann,[2] and Torsten Granzow[3]

[1]*Centre for Nanostructured Media, School of Mathematics and Physics, Queen's University Belfast, Belfast BT7 1NN, United Kingdom*

[2]*IEE S.A., ZAE Weiergewan, 11, rue Edmond Reuter, L-5326 Contern, Luxembourg*

[3]*MRT Department, Luxembourg Institute of Science and Technology (LIST), 4362 Esch-sur-Alzette, Luxembourg*

(Received 8 April 2019; revised manuscript received 10 October 2019; published 8 November 2019)

Ferroelectrics have been rarely considered as suitable candidates for the design of agile devices in the booming field of millimeter wavelengths and terahertz applications. Here a specifically designed free-space quasioptical system to determine the dielectric tunability and losses of a barium titanate single crystal at different temperatures is described. The values obtained are promising to establish ferroelectrics in the inventory of functional materials relevant at millimeter wavelengths. The potential for application of Landau's theory and a discussion of the role of phonon modes on the tunability is presented.

DOI: 10.1103/PhysRevB.100.184104

I. INTRODUCTION

The emerging use of new frequency bands at millimeter-wave frequencies (30–300 GHz) [1] has triggered renewed interest in the properties of functional materials in this range. Among those, ferroic materials such as ferromagnets or ferroelectrics have advantages in applications requiring tunability, as they combine exceptional tuning speed, low power consumption, and a large tuning range [2]. However, their dielectric properties in the millimeter-wave range are still largely unknown, due partly to the presupposition that the high losses observed in polycrystalline ferroelectrics in the microwave range will extend to higher frequencies.

The prototypical ferroelectric barium titanate ($BaTiO_3$, BTO) is of the tetragonal perovskite structure type at room temperature. Its complex dielectric permittivity ε^* has two independent components: (i) the "extraordinary" $\varepsilon^*_{33} = \varepsilon'_{33} + j\varepsilon''_{33}$, with j denoting the imaginary unit, describes the response parallel to the polar axis and (ii) the "ordinary" $\varepsilon^*_{11} = \varepsilon'_{11} + j\varepsilon''_{11}$ is the response orthogonal to it. The permittivity depends on frequency, as various relaxation mechanisms contribute in different frequency ranges [3,4]. Only electrons contribute under high-frequency optical excitation, resulting in fairly low values of $\varepsilon'_{33,\mathrm{elec}} = 5.8$ and $\varepsilon'_{11,\mathrm{elec}} = 5.5$ [5]. With decreasing frequency, various phonon modes start to contribute. Based on Raman or IR spectroscopy, the phonon-dominated ionic permittivity is $\varepsilon'_{33,\mathrm{ph}} = 56$ and $\varepsilon'_{11,\mathrm{ph}} = 1800$–$2200$ [6–10]. These values remain fairly constant until ferroelectric domain wall motion and piezoelectric contributions become relevant below 1 GHz. In polycrystalline ceramics, a dielectric relaxation was observed by several groups at frequencies between 10 and 50 GHz [11–13], and attributed to grain resonances and domain wall vibration [14]. In the case of single crystals, this relaxation is absent.

Upon heating beyond the Curie temperature $T_c \sim 130$ °C, the material undergoes a phase transition from the ferroelectric tetragonal to the paraelectric cubic phase. There is a long-standing discussion as to how much the nature of this transition is of displacive or of the order-disorder type. A displacive phase transition stems from a displacement of atoms from the high-symmetry positions they occupy in the high-temperature phase. The frequency of the phonon mode associated with the primary order parameter decreases to zero at T_c: this is the *soft mode* behavior [15]. On the other hand, during an order-disorder transition it is the frequency of another phonon mode that decreases, the so-called *central mode* [6]. The order-disorder and displacive phase transition models are only limiting cases, and a phase transition usually has characteristics of both, including the cubic-tetragonal phase transition of BTO [16].

The existence of a central mode in addition to the traditional soft mode in BTO was shown by Ponomareva *et al.* using first-principle calculations [17], with experimental evidence for the claim based on far-infrared reflectivity measurements. As these measurements tend to be less reliable at frequencies below 600 GHz, central phonon modes are more typically detected using inelastic spectroscopic techniques such as neutron, Raman, hyper-Raman, or Brillouin scattering. The latter technique in particular was successfully used to track the central peak in barium titanate above the phase transition temperature [18]. Its behavior could be correlated with the anomalous birefringence, piezoelectric effect, and an observed deviation from the Curie-Weiss law [19]. These observations support the results of dielectric spectroscopy in evidencing the existence of the central mode, though its development under an external electric bias field or its influence on properties such as dielectric tunability remain unknown.

In this work we present a method to investigate the dielectric tunability, i.e., the development of the permittivity under an electric field. This method reveals several features that make BTO an interesting candidate as a tunable dielectric for agile applications in the millimeter-wave range: (i) a high permittivity enabling miniaturization of devices, (ii) sufficiently low losses, (iii) the persistence of tunability at high frequencies, and (iv) the phononic origin of the tunability at millimeter wavelengths, suggesting a universal behavior of perovskite-structured ferroelectrics. The tunability is postulated to arise predominantly from changes in the central mode.

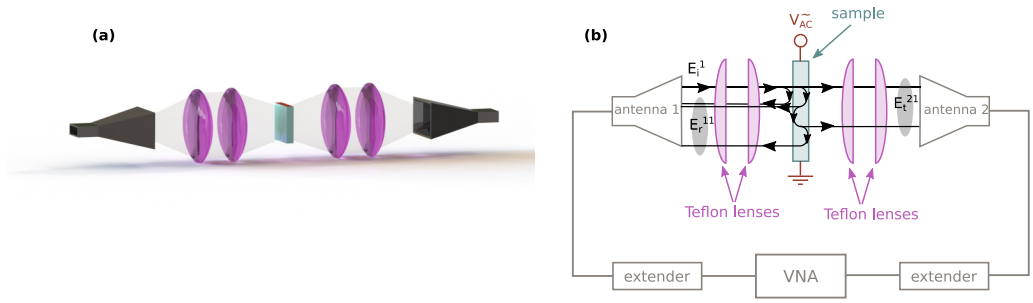

FIG. 1. Dielectric permittivity measurement using a free-space quasioptical setup. (a) Schematic of the experimental setup. (b) Path of the electromagnetic beam in the setup.

II. CHARACTERIZATION OF DIELECTRIC PERMITTIVITY AT MILLIMETER WAVELENGTHS

A. Measurement procedure

Cuboid $BaTiO_3$ single crystals with dimensions of $10 \times 10 \times 1$ mm^3 were obtained from Mateck GmbH (Jülich, Germany), with the sample edges parallel to the crystallographic (001) direction of the pseudocubic perovskite structure. The samples were poled in-plane with polarization along one of the long crystal edges. To apply an electric field, the faces orthogonal to the poling direction were electroded using silver paint and connected to a TREK 20/20C high-voltage power supply. The complex dielectric permittivity ε^* was determined in the frequency range 70–110 GHz, covering the W band, using a free-space quasioptical measurement technique [20]. The setup is schematically depicted in Fig. 1(a). It is based on a vector network analyser (VNA) equipped with frequency extenders. The sample is placed between two horn lens antennas, which transmit the polarized beam into free space, and a set of Teflon lenses that focus the beam onto the sample. The VNA emits a linearly polarized electromagnetic wave; the direction of the wave polarization with respect to the direction of the polar axis of the crystal is adjusted by changing the spatial orientation of the crystal. The scattering parameters (S parameters) of this arrangement are measured, and the amplitudes of the reflected and transmitted electromagnetic wave as functions of frequency were calculated from these S parameters. The temperature of the sample could be controlled by means of a heat gun, with an infrared thermometer at the sample position measuring the actual temperature. This specifically designed experimental setup combines the advantage of the high dynamical range of the VNA needed to measure high permittivity materials with the noncontact nature of the quasioptic setups to apply the bias electric field necessary for the determination of the dielectric tunability.

B. Determination of permittivity

The transmission and reflection spectra for ordinary and extraordinary light polarization, presented for zero external field in Fig. 2, indicate a strong anisotropy of the mm-wave properties. For ordinary light polarization, most of the beam is reflected, resulting in very low transmission. For extraordinary polarization, the levels of reflection and transmission are similar and show oscillations due to Fabry-Perot interferences resulting from repeated reflection of the beam at the different internal sample interfaces as depicted in Fig. 1(b). To obtain the component ε^*_{33} of the complex permittivity, the extraordinary complex refractive index n^*_e was determined by fitting the Fabry-Perot interference fringes, assuming a constant refractive index over the entire frequency range. Because BTO is nonmagnetic, with a magnetic permeability practically equal to 1, n^*_e and ε^*_{33} are related by $\varepsilon^*_{33} = n^{*2}_e$.

1. Fitting Fabry-Perot interference fringes

Taking into account the absorption losses, the transmitted electric field E_t and the reflected electric field E_r can be expressed as

$$\frac{E_t}{E_i} = \frac{t_{12}t_{21}e^{\frac{2\pi}{\lambda}kd}}{1 - r_{12}^2 e^{2(\frac{2\pi}{\lambda}kd - j\frac{2\pi}{\lambda}nd)}} \quad \text{and}$$

$$\frac{E_r}{E_i} = r_{12} + \frac{-t_{12}t_{21}e^{2(\frac{2\pi}{\lambda}kd - j\frac{2\pi}{\lambda}nd)}}{1 - R_{12}^2 e^{2(\frac{2\pi}{\lambda}kd - j\frac{2\pi}{\lambda}nd)}}, \tag{1}$$

with

$$r_{12} = -r_{21} = \frac{1 - n^*}{1 + n^*} = \frac{1 - n^2 - k^2 - 2jk}{(1+n)^2 + k^2}, \tag{2}$$

$$t_{12} = \frac{2(1 + n - jk)}{(1+n)^2 + k^2}, \tag{3}$$

$$t_{21} = \frac{2(n^2 + k^2 + n + jk)}{(1+n)^2 + k^2}, \tag{4}$$

where E_i is the incident electric field, r_{12}, r_{21}, t_{12}, and t_{21} are the complex Fresnel reflection and transmission coefficients at the interface between the air (medium 1) and a dielectric medium (medium 2) of complex refractive index $n^* = n + jk$, R_{12} is the reflection at the air-dielectric interface, d is the thickness of the sample, and λ is the free-space wavelength.

The complex refractive index n^* was determined by fitting simultaneously the lossy Fabry-Perot transmission and reflection coefficients to the experimental data. The starting values for the fit were chosen based on the frequency of the Fabry-Perot oscillations for the real part and by trial and error for the imaginary part. The reliability of this method was ascertained by using $LiNbO_3$ as a test material, for which the dielectric constant is available at these frequencies in the literature [3]. The variance of the two fitting parameters (n and k) indicates that the fitting error is minimal. Therefore, measurement errors are the major source of uncertainty here.

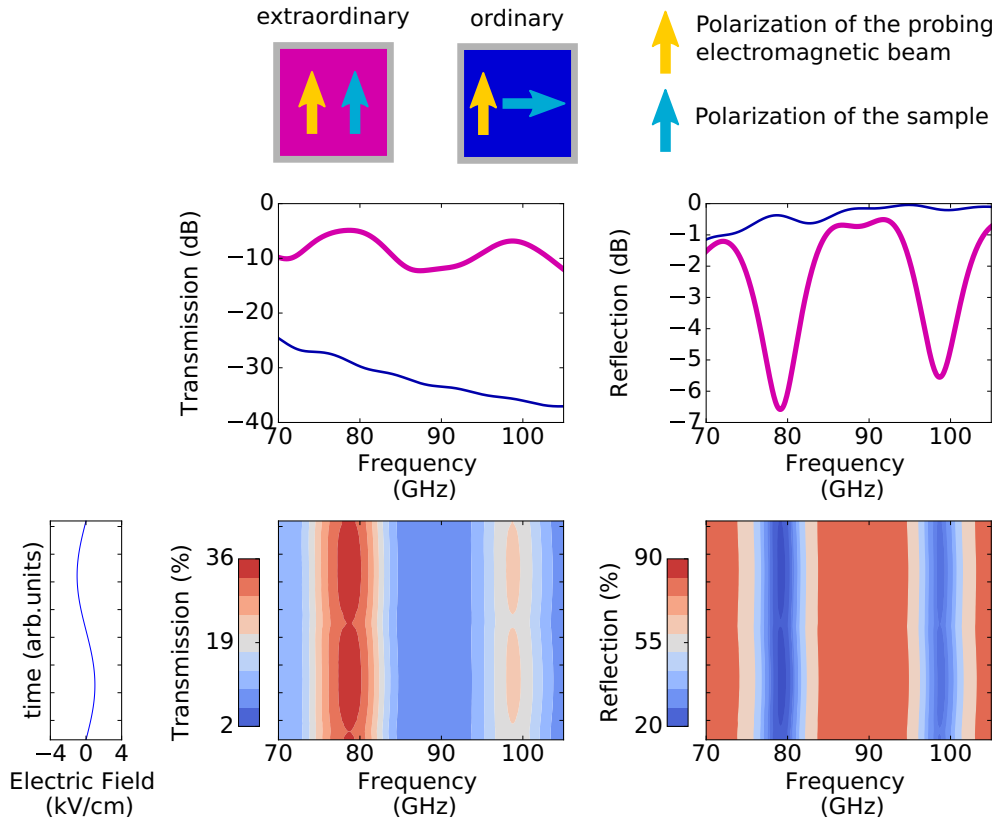

FIG. 2. Transmission and reflection coefficients of BTO at mm wavelengths at room temperature. (Top) Schematic depicting the polarization direction in the extraordinary and ordinary directions. (Bottom) Transmission and reflection coefficients at zero electric field in the extraordinary (thick pink line) and ordinary direction (thin blue line).

Using this method, a value of $\varepsilon^*_{33} = n^{*2}_e = 57.6 + 1.7j$ is obtained. These values correspond very well to [ε_{33}(10 MHz) $\sim$ 56] reported in [21] as well as the values calculated from the phonon contributions ($\varepsilon^{\text{ph}}_{33} \sim 57$) [6]. It is worth noting that the loss tangent $\tan\delta = \varepsilon''/\varepsilon'$ is of the order of 0.03, which is lower than what has been classically observed for ferroelectrics in the microwave range [22] and low enough for technological applications.

The same procedure cannot be applied to determine ε_{11}: the much higher reflectivity of BTO in the ordinary direction, stemming from a dielectric permittivity more than one order of magnitude larger than in the extraordinary direction, prevents the development of significant Fabry-Perot interference fringes. In this case, transmission line theory was used for the evaluation.

2. *Transmission line theory*

Transmission line theory was originally developed to study microwave transmission lines, describing the scattering parameters (S parameters) of a symmetrical two-port network. As a dielectric plate in a free-space experiment can also be considered a two-port network, transmission line theory has been successfully used several times in the past to describe the transmission and reflection of plates of material of a low dielectric constant [23–25]. Although it was developed to address a problem very different from that usually considered with the Fabry-Perot model, the two descriptions are equivalent. Both can be used to model the present free-space experiment.

Assuming a nonmagnetic dielectric slab of thickness d, the scattering coefficients describing the transmitted (S_{21}) and the reflected (S_{11}) signals can be expressed as

$$S_{21}(\omega) = \frac{E_t}{E_i} = \frac{(1 - r_{21}^2)z}{1 - r_{21}^2 z^2}, \tag{5}$$

$$S_{11}(\omega) = \frac{E_r}{E_i} = \frac{(1 - z^2)r_{21}}{1 - r_{21}^2 z^2}, \tag{6}$$

with r_{21} the reflection coefficient defined above and z the transmission coefficient defined as

$$z = \exp -j(\omega/c)\sqrt{\varepsilon}d. \tag{7}$$

Hence, knowing the permittivity of a material, it is possible to calculate the scattering parameters S_{11} and S_{21}. For the inverse process, an estimation is made for the complex permittivity, the value is fed to transmission line theory and the S parameters thus obtained are compared to the experimental results. In the millimeter-wave range, it was shown that the dielectric permittivity is intermediate between the clamped permittivity (ε^T) and the ionic permittivity (ε^{ph}) given by the contribution of the phonon modes. In the case of BTO, the clamped and ionic permittivity values are both reported to be about $\varepsilon'_{11} = 1800$–2200 depending on the references [6–10]. It is thus possible to obtain reasonable estimations for the real part ε_{11}. Comparing the calculated values to the

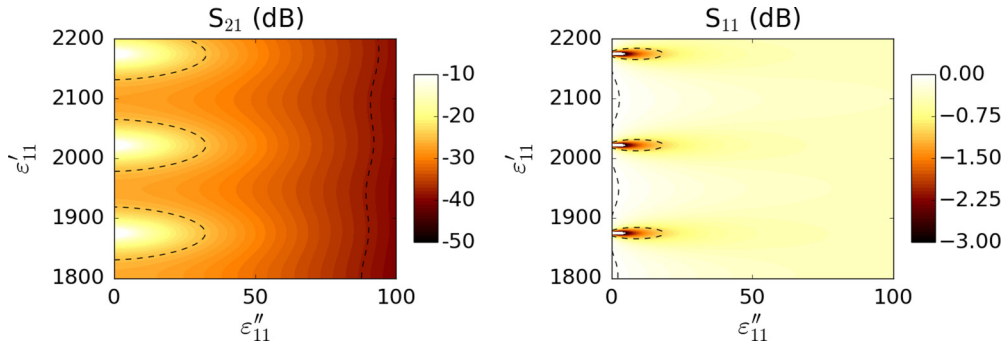

FIG. 3. Scattering parameters S_{11} and S_{21} as a function of ε'_{11} and ε''_{11} at 90 GHz calculated using transmission line theory. The dashed lines indicate the area reproducing the experimental data.

measured values, it is possible to find an area of $(\varepsilon'_{11}, \varepsilon''_{11})$ that reproduces the experimental value. The calculated scattering parameters are presented in Fig. 3. However, as the solutions are not unique, the experimental results can be explained by a range of combinations of $(\varepsilon'_{11}, \varepsilon''_{11})$, reducing the reliability of the actual value of ε^*_{11}. Nonetheless, using the literature-based data of $\varepsilon'_{11} = 2000 \pm 200$, the imaginary part can be estimated to $\varepsilon''_{11} = 50 \pm 50$ from this analysis. In the worst case, the loss tangent is still lower than 0.05. These losses are about the same order of magnitude as characterized in the extraordinary direction, supporting the idea that the losses in the millimeter range are not as high as observed in the microwave range. It is interesting to note that the transmission line theory and Fabry-Perot model give transmission and reflection coefficients that are in perfect agreement, reinforcing the validity of the approach (Fig. 4).

Hence, the quasioptical free-space setup enables the determination of the extraordinary complex permittivity ε^*_{33}. As this value is similar to the one measured at phonon frequencies, it shows the absence of relaxation down to the W band. With the knowledge of the absence of relaxation and an estimation of ε'_{11} from high frequency measurements, an order of magnitude of the losses ε''_{11} can be evaluated.

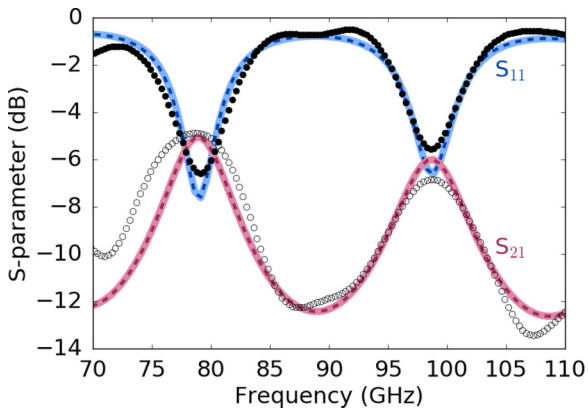

FIG. 4. Comparison between the transmission line theory, the Fabry-Perot fringes modeling and the experimental results. Experimental results are represented with circles (S_{11}: full symbols and S_{21}: open symbols). The full lines depict the S parameters calculated with the transmission line theory, while the dashed lines the ones calculated using Fabry-Perot interference fringes.

III. EXPERIMENTAL DETERMINATION OF ELECTRICAL TUNABILITY

An additional capability made possible by the noncontact nature of the characterization method presented here is the possibility to study the dielectric tunability as a function of temperature. In Sec. III A the method to determine the dielectric tunability is presented. This method is further applied in Sec. III B to discuss the evolution of tunability with temperature.

A. Room-temperature measurements

When an electric field of up to $E_{\text{ext}} = 3$ kV/cm is applied to the sample, the transmission and reflection spectra for extraordinary light polarization change. This is evidenced in Figs. 5(a) and 5(b) by the color variation along the vertical axis. The elongated eight shapes at about 80 and 100 GHz indicate that both the amplitude and the width of the interference fringes varies with the electric field. A similar effect is not observed for ordinary light polarization.

It is important to note that the change in the Fabry-Perot pattern need not be due exclusively to a change in the permittivity: the thickness of the BTO samples changes due to the converse piezoelectric effect which itself changes the optical path effectively changing the transmission and reflection coefficients. It is therefore necessary to differentiate between a change in thickness and a change in the permittivity by modifying the thickness of the sample in Eqs. (1)–(4) for each electric field using the piezoelectric coefficient $d_{31} = -34$ pm/V [9]. Figure 5(c) shows the real part ε'_{33} of the permittivity as well as the loss tangent $\tan\delta$ determined in this way. Both quantities show the usual butterfly hysteresis shape. The relative tunability of the permittivity $\nu_r = \frac{\varepsilon'(0)-\varepsilon'(E_{\max})}{\varepsilon'(0)}$ reaches values of 0.3% to 0.4% at a field of 3 kV/cm. While this value at first appears to be rather small, it should be kept in mind that only a low electric field could be applied due to the large sample size required by the free-space geometry. In practical applications involving thin-film geometry, the material is subject to a much higher field.

As already mentioned, the contribution of a piezoelectric deformation to the measured spectra was already taken into account and compensated for here. To evaluate how large this contribution actually is, Fig. 6 compares the influence of the piezoelectric and dielectric contribution on the transmission

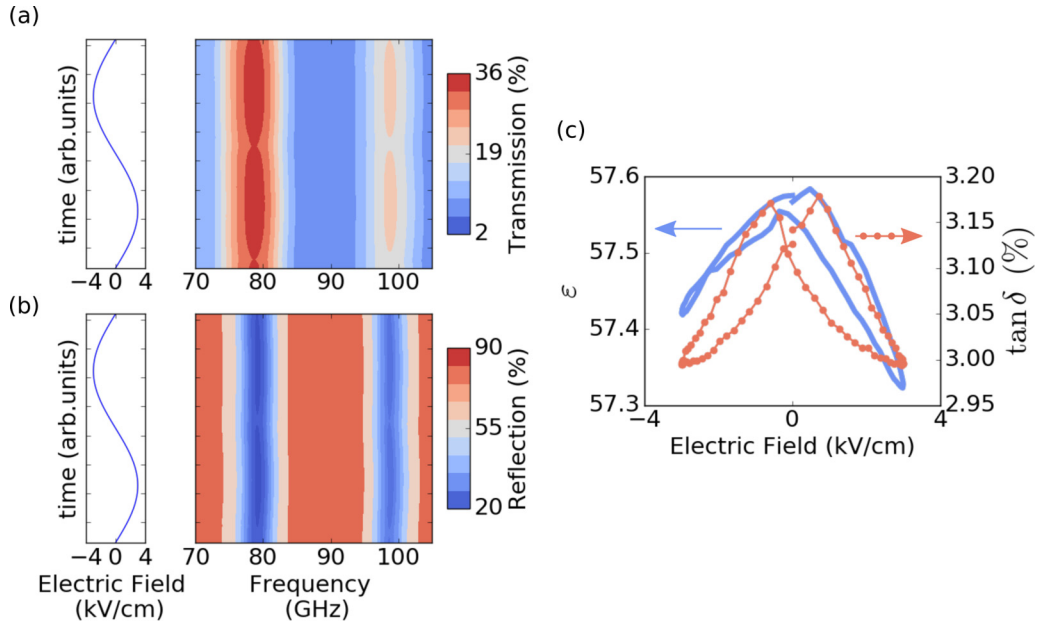

FIG. 5. Influence of electric field on the dielectric properties of BTO at mm wavelengths. Experimentally observed evolution of (a) transmission and (b) reflection coefficients as a function of bias electric field. (c) The change in the real part of permittivity ε'_{33} and loss tangent $\tan\delta_{33}$ determined from these measurements and assumed constant in the frequency range considered.

coefficient. If only a piezoelectric thickness change is taken into account, the expected change in transmission is about one order of magnitude lower than what is experimentally observed. This indicates that the determination of the relative dielectric tunability is reliable, even if the accounting for piezoelectric contributions should not be entirely correct.

B. Temperature dependence of tunability

The evolution of the transmission spectrum for extraordinary light polarization as a function of temperature is presented in Fig. 7(a). For reasons of clarity, the scattering parameter $S_{12} = 10\log(\mathcal{T})$ is displayed, where $\mathcal{T}$ is the transmission coefficient. With increasing temperature, there is a continuous decrease in the transmission coefficient as well as the frequency of the Fabry-Perot interference fringes. At the Curie temperature around 400 K, a strong drop in transmission indicates the sudden increase of permittivity at the transition to the paraelectric phase. Above this temperature, the interference fringes practically disappear, making an evaluation of the permittivity impossible. The evolution of the permittivity in the W band as a function of temperature is presented in Fig. 7(c) alongside the value measured at 10 MHz using a dielectric spectrometer. The fact that the evolution of the permittivity is very similar at these very different frequency ranges indicates the absence of additional dielectric relaxations down to the low frequency range and attests to the robustness of the measurement.

Application of an external field leads to a shift of the Fabry-Perot pattern at each temperature, from which the field dependence of the permittivity ε'_{33} can be calculated as described above. The resulting butterfly loops are exemplarily shown for four temperatures in Fig. 7(b) along with the relative tunability ν_r, which increases with temperature.

The temperature dependence of the tunability develops parallel to that of the permittivity as can be seen in Fig. 7(c). This can be fully expected from Landau's theory, as will be discussed further in the following section.

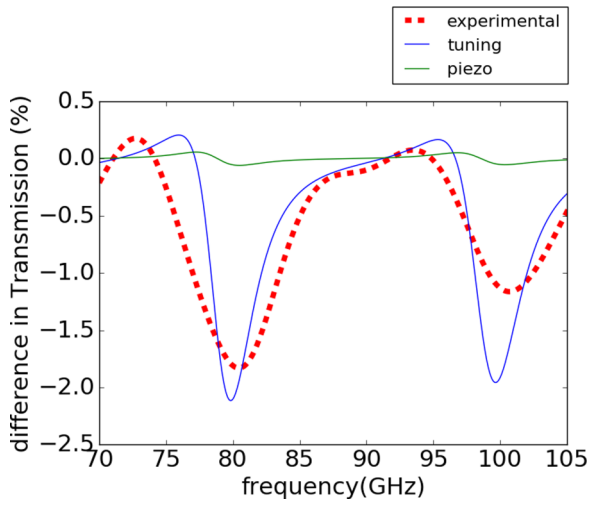

FIG. 6. Comparison of the change in the transmission coefficient experimentally observed (red dashed line), due to the change in thickness owing to the piezoelectric response (green line) and due to the dielectric tuning mechanism (blue line). For each frequency the difference between the transmission coefficient at zero electric field and at the largest electric field is plotted.

IV. DISCUSSION OF FERROELECTRIC TUNABILITY AT MILLIMETER WAVELENGTHS

In this section it is exemplified how the measurements of dielectric permittivity and tunability can be valuable for future pursuit of the understanding of the physics of ferroelectrics.

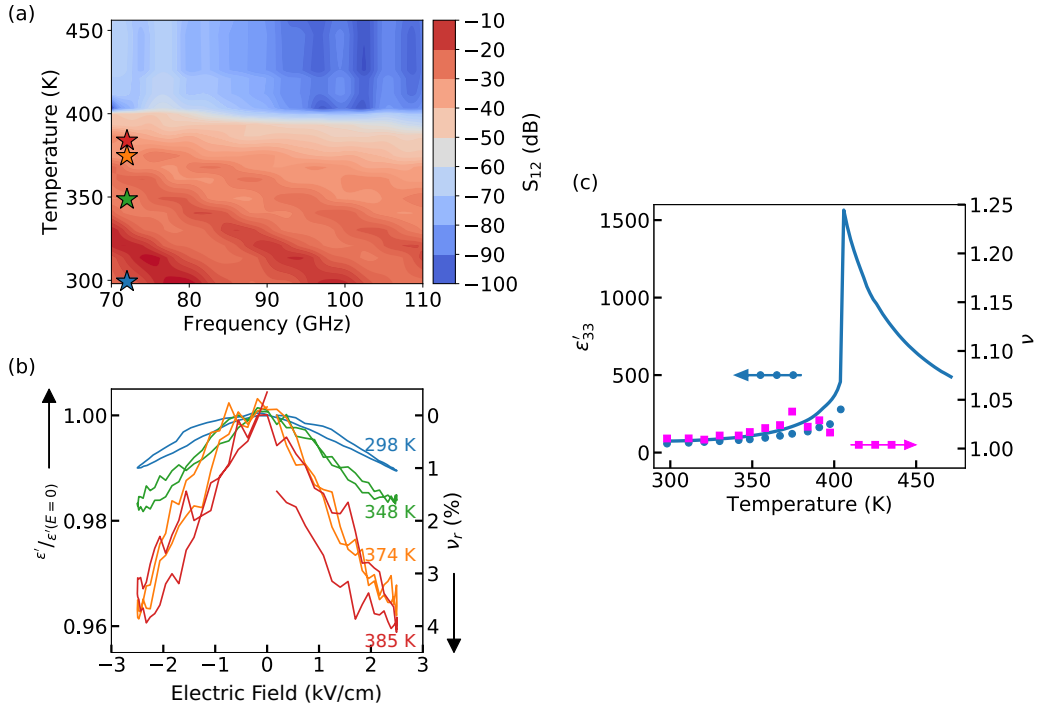

FIG. 7. Influence of temperature on the dielectric permittivity and tunability of BTO single crystals. (a) Evolution of the scattering parameter $S_{12} = 10\log(T)$ in the extraordinary direction as a function of frequency and temperature. The stars denote the temperatures at which the hysteresis curves presented in (b) were measured. (b) ε'_{33} and ν_r as a function of E at four different temperatures. (c) Comparison of the permittivity ε'^{S}_{33} measured at 10 MHz (full line) and permittivity measured at mm wavelengths (blue circles). The evolution of the tunability (ν) with temperature is also presented (pink squares).

A. Phenomenological model based on Landau theory

Based on Landau's theory, Tagantsev *et al.* [26] successfully described the evolution of the real part of the dielectric constant under an electric field E with the relationship

$$\varepsilon'(E) = \frac{\varepsilon'(E=0)}{1 + 3\beta[\varepsilon'(E=0)\varepsilon_0]^3 E^2}, \tag{8}$$

where ε_0 is the permittivity of vacuum, $\varepsilon'(E=0)$ is the dielectric constant at zero bias field, and β is a Landau coefficient. The full derivation of this equation from Landau's theory can be found in Refs. [27,28]. Of particular interest in the context of this study is the possibility to use Landau's theory to estimate the high-field tunability of BTO at a fixed temperature. The room-temperature coefficients $\beta = 8 \times 10^{13}$ J C^4 m^5 and $\varepsilon'(E=0) = 57.7$ can be determined by fitting the nonswitching part of the ε-E loop (Fig. 8). β is larger than reported at low frequencies [30], an effect of the limited number of processes contributing to the high-frequency permittivity and the resulting much lower value of $\varepsilon(E=0)$. The evolution of ε' and the relative tunability ν_r with electric field thus estimated are presented in Fig. 5(d). Under a bias field of 20 kV/cm, the relative tunability of BTO is estimated to 11%. Due to the absence of dipolar contributions at millimeter wavelengths, the relative tunability is lower than what was reported at lower frequencies ($\leqslant$30% [31,32] at 1 kHz). Still, this value of relative tunability is significant, especially considering the limited losses.

Equation (8) predicts that tunability should scale with permittivity, which is in good agreement with Fig. 7(c). Though the data on tunability is quite noisy, it can still be observed that tunability and permittivity follow the same trend. Thus, bringing the phase transition closer towards room temperature is a viable strategy for increasing the tunability at mm wavelengths.

The extrapolation of results to higher field must be taken with caution considering the limited range of electric field available here. Therefore, these measurements show a quantitative agreement with the predictions of Landau theory concerning the temperature development, but further research is necessary to obtain quantitative information on the tunability.

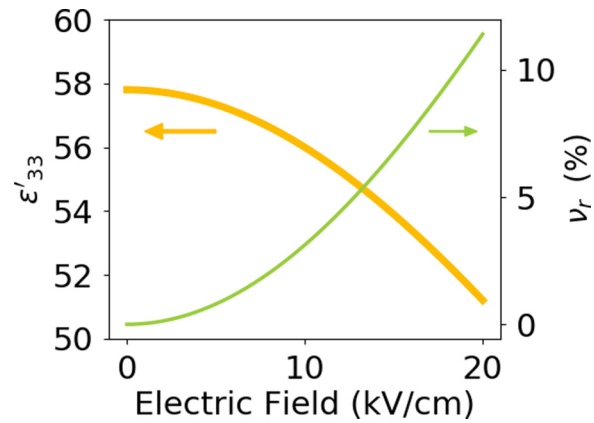

FIG. 8. Evolution of the permittivity ε'_{33} and relative tunability ν_r as a function of electric field based on Eq. (8), with $\varepsilon'(E=0) = 57.7$ and $\beta = 8 \times 10^{13}$ J C^4 m^5 (See Supplemental Material [29].).

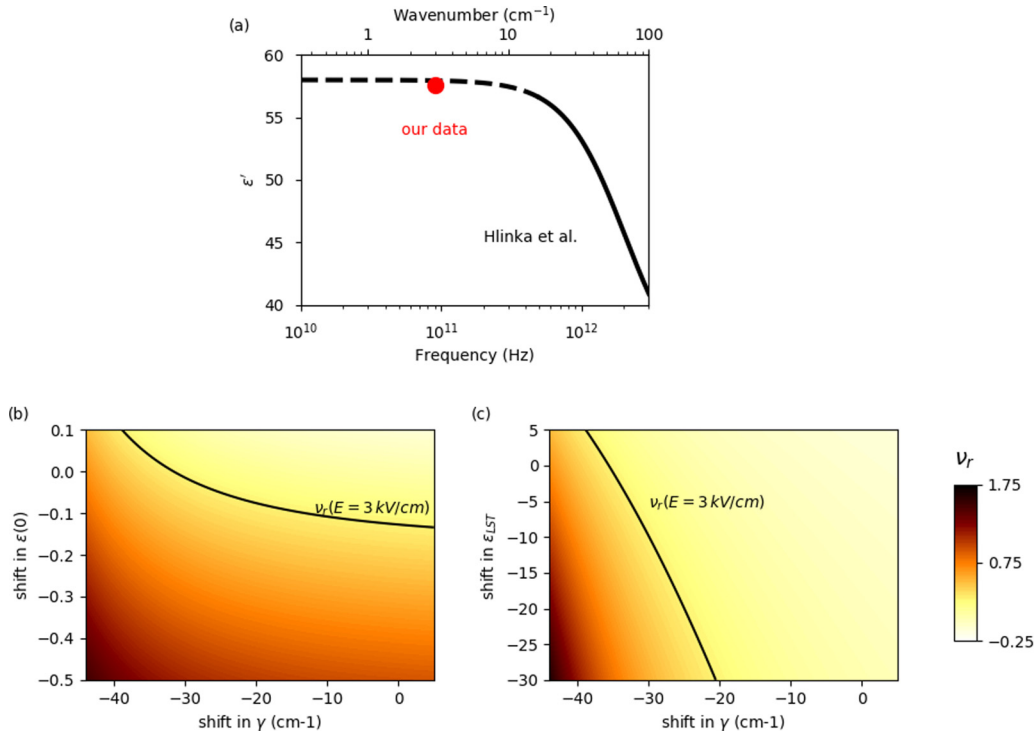

FIG. 9. Simulation of the dielectric permittivity at millimeter wavelengths and THz frequencies. (a) Dielectric dispersion modeled by the Debye relaxation proposed by Hlinka *et al.* [16] (full line). The dashed line is the extension to lower frequencies, the circle denotes the zero-field value obtained in this work. (b) and (c) Relative tunability ν_r (%) at 100 GHz with variation of the Debye parameters $\varepsilon(0)$, $\varepsilon_{\mathrm{LST}}$, and γ. The black line represents the tunability $\nu_r = 0.3\%$ observed in this work at the maximum field of 3 kV/cm.

B. Discussion on phonon modes contribution

At millimeter wavelengths, dielectric tunability can arise solely from changes in the ionic or electronic contribution to the permittivity. As the electro-optic effect in BTO, representing the electronic contributions, is low [21], the ionic response, i.e., the electric-field dependence of phonons, can be considered the main contributing factor The question now is which phonon modes bear responsibility for the dielectric tunability at millimeter wavelengths.

Investigations at terahertz frequencies indicated that tunability in incipient bulk ferroelectrics $SrTiO_3$ (STO) [33] and $KTaO_3$ (KTO) [34] originates from the hardening of the soft mode. These results were reproduced by first-principles-based molecular-dynamics simulations [35]. Additionally, these simulations revealed that in the case of strained STO films, the tunability emanates from the hardening of the soft mode and central mode as well as a change in the coupling between these two modes. To investigate what could be the origin of tunability in BTO, the modeling of the frequency dispersion of the dielectric constant and examination of the influence of the various parameters on this model is a first step.

Hlinka *et al.* used an expanded Debye relaxation [16] to account for the dielectric contribution of the central mode to the permittivity in the THz range:

$$\varepsilon'(f) = \varepsilon'_{\mathrm{LST}} + \frac{\Delta\varepsilon'}{1 - i2\pi f/\gamma}, \tag{9}$$

where f is the frequency, $\gamma = 68\ \mathrm{cm}^{-1} = 12.8$ THz is the Debye frequency, $\varepsilon'_{\mathrm{LST}} = 33$ is the Lyddane-Sachs-Teller dielectric contribution, and $\Delta\varepsilon'$ is the dielectric step defined as $\Delta\varepsilon' = \varepsilon'(0) - \varepsilon'_{\mathrm{LST}} = 24.5$. $\varepsilon'_{\mathrm{LST}}$ takes into account all high frequency contributions including the electronic permittivity and the contributions of all phonon modes except the central mode. It also includes the soft mode contribution. Far from the central mode, its influence on the permittivity is dominated by the dielectric step $\Delta\varepsilon'$. Figure 9(a) shows ε' as determined from Eq. (9), extrapolating from the frequency range considered by Hlinka *et al.* to lower frequencies. The value of $\varepsilon'(E = 0) = 57.7$ determined in Sec. III above is very well described by the relation, justifying the use of the model down to millimeter wavelengths.

In the frame of this model, changes in the permittivity, and thus the experimentally observed electric-field-induced tunability, arise from changes in the Debye relaxation of the central mode. To estimate the influence each of the parameters in Eq. (9) has on the tunability, the numerical values of γ, $\varepsilon'_{\mathrm{LST}}$, and $\varepsilon'(0)$ were continuously varied from the zero-field values proposed by Hlinka *et al.* [16]. Figures 9(b) and 9(c) shows the relative tunability based on these simulations, with the experimentally observed tunability at 3 kV/cm shown as a continuous line. It can be seen that if the other parameters are kept unchanged, a shift in γ by $-30\ \mathrm{cm}^{-1}$ or 44% of its zero-field value is required to account for the observed tunability. The same tunability could be accomplished by a change of -0.12 in $\varepsilon'(0)$, i.e., 0.21% of the zero-field value. At the same time, $\varepsilon'_{\mathrm{LST}}$ would have to decrease from 33 to -50, a clearly unphysical result. Even if a combination of all three parameters is changed, the influence of changes in $\varepsilon'_{\mathrm{LST}}$ are far too low to outweigh the other parameters. Apparently, changes

in $\varepsilon'_{\mathrm{LST}}$ play no significant role in the tunability. We suggest that the dielectric tunability in BTO arises predominantly from change in the dielectric step $\Delta\varepsilon'$, i.e., a change in $\varepsilon'(0)$, possibly in combination with a change in γ. Since the model describes the Debye relaxation associated with the central mode and since the central mode and soft mode are coupled in BTO, a contribution of a field-induced change in this coupling to the changes in the Debye relaxation cannot be excluded. Further studies focusing on the influence of electric field in the terahertz and infrared range would be necessary to provide a definitive conclusion.

V. SUMMARY

In this work the properties of the model ferroelectric barium titanate were investigated at millimeter wavelengths. Its dielectric permittivity and its evolution under bias electric field were measured. It is shown that in this frequency range only the ionic and electronic polarization contributes to the dielectric response; the corollary being that the dielectric tunability arise from a change in one of these contributions. Additionally, the interest of our measurements in the context of Landau's theory was explored and the influence of the central mode on the observed tunability was discussed.

The high permittivity of BTO, its limited losses, and its tunability under electric field exposed in this work are three arguments in favor of the use of BTO in devices for agile applications at millimeter wavelengths. Therefore, this article presents a number of building blocks that proves the potential of ferroelectrics in tomorrow's technology and an indisputable need to carry on further research in this field.

ACKNOWLEDGMENTS

This work was supported by the National Research Fund, Luxembourg (FNR/C13/MS/5817287 and FNR/Midimat/10036216) and US-Ireland R&D Partnership Programme (Grant No. USI 120).

[1] F. C. Commission, Use of Spectrum Bands Above 24 GHz for Mobile Radio Services, GN Docket No. 14-177, Notice of Proposed Rulemaking, 15 FCC Record 138A1, Tech. Rep. (2015).
[2] S. Gevorgian, *Ferroelectrics in Microwave Devices, Circuits and Systems* (Springer, London, 2009).
[3] C. Cochard, T. Spielmann, N. Bahlawane, A. Halpin, and T. Granzow, J. Phys. D: Appl. Phys. **50**, 36LT01 (2017).
[4] C. Cochard, M. Guennou, T. Spielmann, N. van Hoof, A. Halpin, and T. Granzow, J. Appl. Phys. **123**, 154105 (2018).
[5] M. S. Shumate, Appl. Phys. Lett. **5**, 178 (1964).
[6] J. Petzelt, Ferroelectrics **375**, 156 (2008).
[7] Y. Luspin, J. L. Servoin, and F. Gervais, J. Phys. C: Solid State Phys. **13**, 3761 (1980).
[8] O. Nakao, K. Tomomatsu, S. Ajimura, A. Kurosaka, and H. Tominaga, Appl. Phys. Lett. **61**, 1730 (1992).
[9] B. Jaffe, W. R. Cook Jr., and H. Jaffe, *Piezoelectric Ceramics* (Academic Press, London and New York, 1971).
[10] A. Scalabrin, A. S. Chaves, D. S. Shim, and S. Porto, Phys. Status Solidi **79**, 731 (1977).
[11] T. Tsurumi, J. Li, T. Hoshina, H. Kakemoto, M. Nakada, and J. Akedo, Appl. Phys. Lett. **91**, 182905 (2007).
[12] T. Teranishi, T. Hoshina, H. Takeda, and T. Tsurumi, IEEE Trans. Ultrason. Ferroelectr. Freq. Control **57**, 2118 (2010).
[13] S. Kazaoui, J. Ravez, M. Maglione, and P. Goux, Ferroelectrics **126**, 203 (1992).
[14] L. Jin, V. Porokhonskyy, and D. Damjanovic, Appl. Phys. Lett. **96**, 242902 (2010).
[15] J. F. Scott, Rev. Mod. Phys. **46**, 83 (1974).
[16] J. Hlinka, T. Ostapchuk, D. Nuzhnyy, J. Petzelt, P. Kuzel, C. Kadlec, P. Vanek, I. Ponomareva, and L. Bellaiche, Phys. Rev. Lett. **101**, 167402 (2008).
[17] I. Ponomareva, L. Bellaiche, T. Ostapchuk, J. Hlinka, and J. Petzelt, Phys. Rev. B **77**, 012102 (2008).
[18] J.-H. Ko, S. Kojima, T.-Y. Koo, J. H. Jung, C. J. Won, and N. J. Hur, Appl. Phys. Lett. **93**, 102905 (2008).
[19] J.-H. Ko, T. H. Kim, K. Roleder, D. Rytz, and S. Kojima, Phys. Rev. B **84**, 094123 (2011).
[20] C. Cochard, T. Spielmann, M. K. Matters-Kammerer, A. R. van Dommele, A. Halpin, J. Gomez-Rivas, and T. Granzow, in *2016 41st Int. Conf. Infrared, Millimeter, Terahertz waves* (IEEE, Washington, DC, 2016), pp. 1–2.
[21] M. Zgonik, P. Bernasconi, M. Duelli, R. Schlesser, P. Günter, M. H. Garrett, D. Rytz, Y. Zhu, and X. Wu, Phys. Rev. B **50**, 5941 (1994).
[22] D. Nuzhnyy, J. Petzelt, M. Savinov, T. Ostapchuk, V. Bovtun, M. Kempa, J. Hlinka, V. Buscaglia, M. T. Buscaglia, and P. Nanni, Phys. Rev. B **86**, 014106 (2012).
[23] J. Krupka, Meas. Sci. Technol. **17**, R55 (2006).
[24] A. M. Nicolson and G. F. Ross, IEEE Trans. Instrum. Meas. **19**, 377 (1970).
[25] W. B. Weir, Proc. IEEE **62**, 33 (1974).
[26] A. K. Tagantsev, V. O. Sherman, K. F. Astafiev, J. Venkatesh, and N. Setter, J. Electroceram. **11**, 5 (2003).
[27] M. E. Lines and A. M. Glass, *Principles and Applications of Ferroelectrics and Related Materials* (Oxford University Press, Oxford, 1977).
[28] P. Chandra and P. B. Littlewood, Top. Appl. Phys. **105**, 69 (2007).
[29] See Supplemental Material at http://link.aps.org/supplemental/10.1103/PhysRevB.100.184104 for description of the models considered.
[30] Y. L. Wang, A. K. Tagantsev, D. Damjanovic, N. Setter, V. K. Yarmarkin, A. I. Sokolov, and I. A. Lukyanchuk, J. Appl. Phys. **101**, 104115 (2007).
[31] M. Budimir, D. Damjanovic, and N. Setter, Appl. Phys. Lett. **88**, 082903 (2006).
[32] L. Curecheriu, M. T. Buscaglia, V. Buscaglia, Z. Zhao, and L. Mitoseriu, Appl. Phys. Lett. **97**, 242909 (2010).
[33] V. Skoromets, F. Kadlec, C. Kadlec, H. Němec, I. Rychetsky, G. Panaitov, V. Müller, D. Fattakhova-Rohlfing, P. Moch, and P. Kužel, Phys. Rev. B **84**, 174121 (2011).
[34] V. Skoromets, C. Kadlec, H. Němec, D. Fattakhova-Rohlfing, and P. Kužel, J. Phys. D. Appl. Phys. **49**, 065306 (2016).
[35] J. Weerasinghe, D. Wang, and L. Bellaiche, J. Phys.: Condens. Matter **25**, 252202 (2013).